CrystEngComm

Unusual Single Crystal to Single Crystal Phase Transition of a Nicotine Salt Monitored Using Temperature Dependent Single Crystal X-ray Diffraction

Journal:	*CrystEngComm*
Manuscript ID	CE-COM-01-2023-000042.R1
Article Type:	Communication
Date Submitted by the Author:	06-Mar-2023
Complete List of Authors:	Angevine, Devin; University at Buffalo College of Arts and Sciences, Chemistry Department Mitchell, Travis; University at Buffalo College of Arts and Sciences, Chemistry Zhang, Xiaotong; University at Buffalo College of Arts and Sciences, Chemistry Benedict, Jason; University at Buffalo College of Arts and Sciences, Chemistry Department

COMMUNICATION

Unusual Single Crystal to Single Crystal Phase Transition of a Nicotine Salt Monitored Using Temperature Dependent Single Crystal X-ray Diffraction

Received 00th January 20xx,
Accepted 00th January 20xx

DOI: 10.1039/x0xx00000x

Devin J. Angevine,[a] Travis Mitchell,[a] Xiaotong Zhang,[a] & Jason B. Benedict *[a]

Abstract: The organic salt (S)-nicotinium 2,6-dihydroxybenzoate undergoes reversible single crystal to single crystal phase transition at 104 K. The phase transition was monitored using temperature dependent single crystal X-ray diffraction and was attributed to symmetry breaking translations and rotations of the crystal components.

It is estimated that nicotine is the second most consumed active pharmaceutical ingredient (API) with approximately 1.3 billion smokers worldwide and a recent sharp rise in vaping product usage.[1] Despite this widespread use, nicotine is known to undergo a variety of undesirable reactions under ambient conditions including oxidation from atmospheric oxygen, thermal decomposition, and ultraviolet (UV) radiation induced degradation.[2-5]. Upon prolonged exposure to UV irradiation, nicotine degrades into a variety of compounds including nicotinic acid, oxynicotine, and methylamine. While some degradation products such as nicotinic acid do not possess health hazards, other by-products such as methylamine may have further unwanted downstream effects and with greater risk.[6, 7] To alleviate such issues associated with API degradation, the solid-state is often targeted through formulation methods, such as crystal engineering.[8-10] Co-crystal engineering and salt formation, a method in which an API non-covalently interacts with a coformer or salt former, allows for the tuning of properties while also maintaining the biological function of the API.

Sensitive APIs such as nicotine or APIs with issues such as limited solubility may need specialized manufacturing methods. One such method, spray freezing into liquid (SFL), can be utilized with various solvent systems at ultra-low cryogenic temperatures to capture frozen particles of an API which are then dried into a powdered form.[11] With cryogenic processes as this, it is crucial to understand the behavior of these materials under conditions that may be encountered during manufacturing.

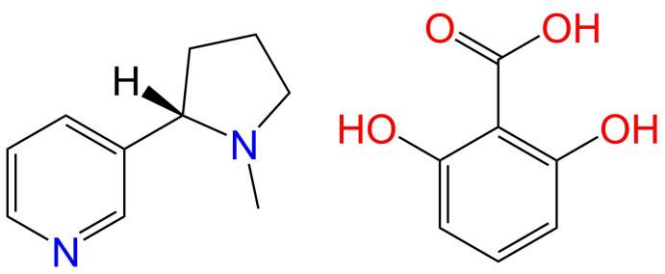

Scheme 1: Chemical structures of the API (S)-nicotine (left) and the salt former 2,6-dihydroxybenzoic acid (left)

Recently co-crystal engineering has been applied to nicotine to alleviate the degradation issues that are associated with this API. Nicotine appears to be particularly amenable to crystallization methods as a multitude of solid-state materials have been reported, including both co-crystals and salts. Capucci et al. synthesized a series of halogenated nicotine co-crystals.[12] Though unsuitable for human consumption, these co-crystals demonstrated the ability to isolate the API in the solid-state.

To make these solid-state nicotine formulations suitable for human consumption, safer materials must be utilized as the coformer or salt former. To this end, a series of nicotine salts were previously reported utilizing salt former molecules that the US FDA certifies as generally recognized as safe (GRAS).[13] These materials utilized forms of malic acid, orotic acid, and gentisic acid to synthesize safer nicotine salts.[14-16] In addition, these nicotine salts also possessed enhanced and tunable thermal properties with significantly improved photostability.

To build upon this work, 2,6-dihydroxybenzoic acid (2,6-DHBA) was selected as a suitable former to combine with nicotine. 2,6-DHBA is commonly found in foods such as beer,

[a] *Department of Chemistry, University at Buffalo, Natural Sciences Complex, Buffalo, NY 14260-3000, USA*
**Corresponding Author: jbb6@buffalo.edu*
*Electronic supplementary information (ESI) available. CCDC Deposition number 2233083 (**HT salt**) & 2233084 (**LT salt**). For ESI and crystallographic data in CIF or another electronic format see DOI: 10.1039/ x0xx00000x*

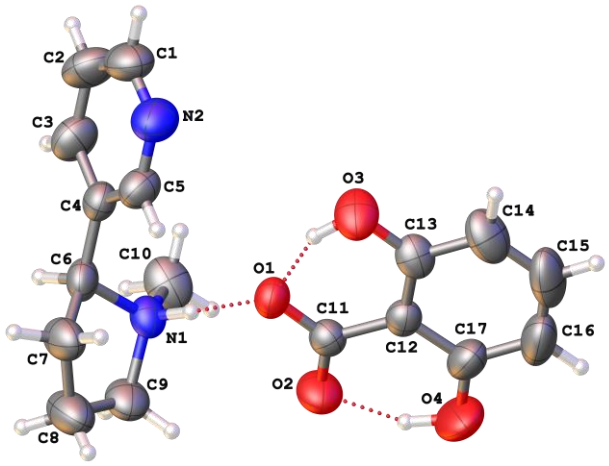

Figure 1: Asymmetric unit of (S)-nicotinium 2,6-dihydroxybenzoate at room temperature (**HT salt**). Atom colors: oxygen (red), nitrogen (blue), carbon (grey), hydrogen (white). Hydrogen bond interactions are highlighted with red dashed lines. Appropriate atomic labels are shown.

strawberries and olives.[17] In addition, 2,6-DHBA has a pK_a of 1.51 while nicotine has a pK_{a1} of 8.02, leading to a ΔpK_a of 6.51. With such a high ΔpK_a, the proton transfer required to form a salt may be reasonably be expected.[18]

When 2,6-DHBA and (S)-nicotine were combined in ethanol in a one-to-one stoichiometric ratio, the corresponding one-to-one salt (S)-nicotinium 2.6-dihydrozybenzoate was crystallized using slow evaporation. Simulated crystal habits were in good agreement with indexed faces (Figure S17).[19, 20] Analysis via single crystal X-ray diffraction (SC-XRD) under ambient conditions at 293 K indicated that the salt (**HT salt**) crystallized in the monoclinic space group $P2_1$. The asymmetric unit consists of a protonated nicotine (nicotinum) and a deprotonated 2,6-dihydroxybenzoic acid (2,6-dihydroxybenzoate; 2,6-DHB). Two *S*(6) intramolecular hydrogen bond interactions were observed between each of the hydroxyl groups and one of the oxygens of the carboxylate (Figure 1). The O-H---O interaction distances between these oxygen atoms were 2.527(3) Å and 2.522(4) Å. A *D* type hydrogen bonding interaction corresponding to the proton transfer was observed between the nicotinium and the 2,6-dihydroxybenzoate with a distance of 2.699(3) Å between heteroatoms. When viewed down [100], the hydrogen bonded ion pairs of the **HT salt** form columns parallel to [010] (Figure S3). The columns intercalate with neighboring columns along [001] to produce 2D-sheets. These 2D-sheets stack along [100] to produce the bulk crystal structure (Figure S4).

Upon cooling the crystal from room temperature down to 90 K, a significant increase in the number of reflections was observed suggesting single crystalline phase transition. While the symmetry of the new cell (**LT salt**) remained monoclinic $P2_1$, the *a*- and *c*-axes increased from 7.7196(5) Å and 9.4241(6) Å to 9.9691(4) Å and 13.8196(5) Å, respectively. The β angle also exhibited a marked change from 108.980(2)° to 101.995(1)°. The length of the *b*-axis remained relatively invariant (11.7045(7) Å vs. 11.5520(4) Å) after the phase transition. Together these changes produced an approximate doubling of the volume which increased from 805.21(9) $Å^3$ to 1556.8(1) $Å^3$. Precession images confirmed a near doubling of the total observed reflections (Figures S18 & S19, Tables S1 & S2). The cell transformation necessitated a reinvestigation of the morphology, the results of which were in good agreement with the redetermined calculated habit (S17).

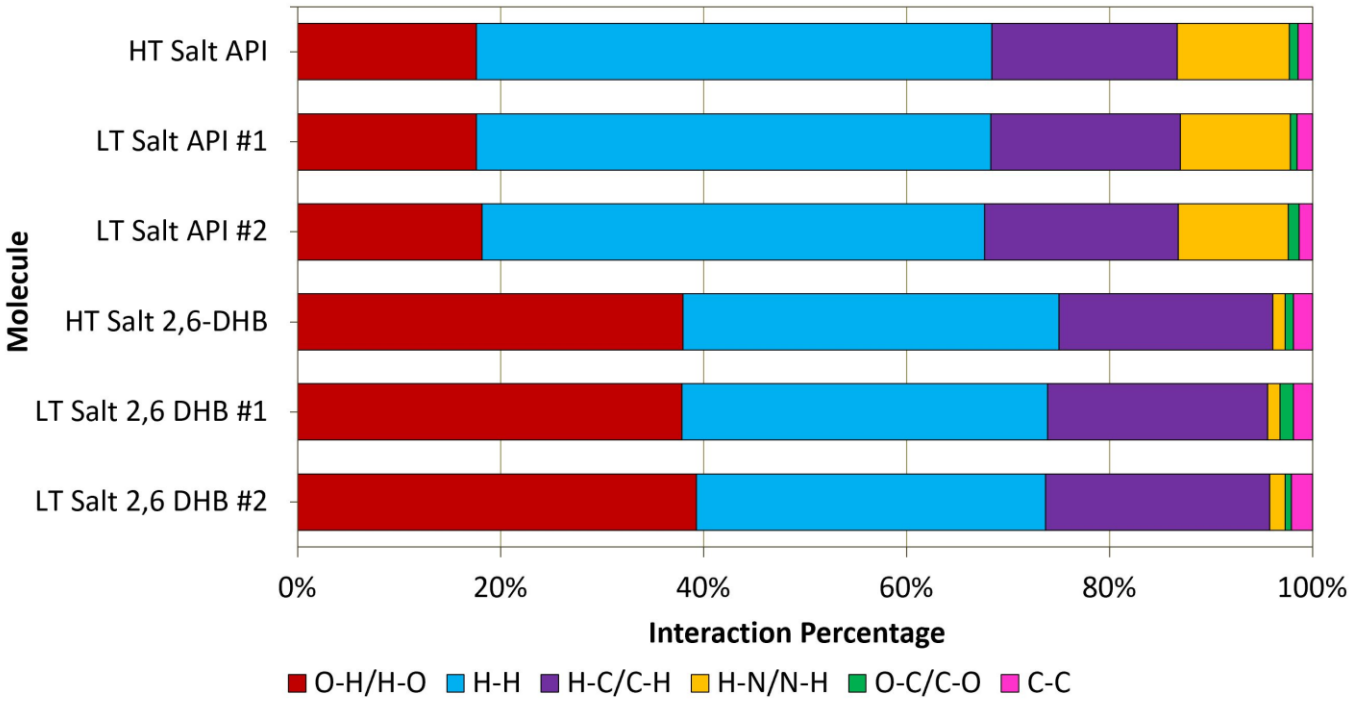

Figure 2: Interaction types and percentages for the API and 2,6-DHB molecules in the **HT salt** and **LT salt**. All percentages were acquired through Hirshfeld surface calculations using *Crystal Explorer 17.5*.

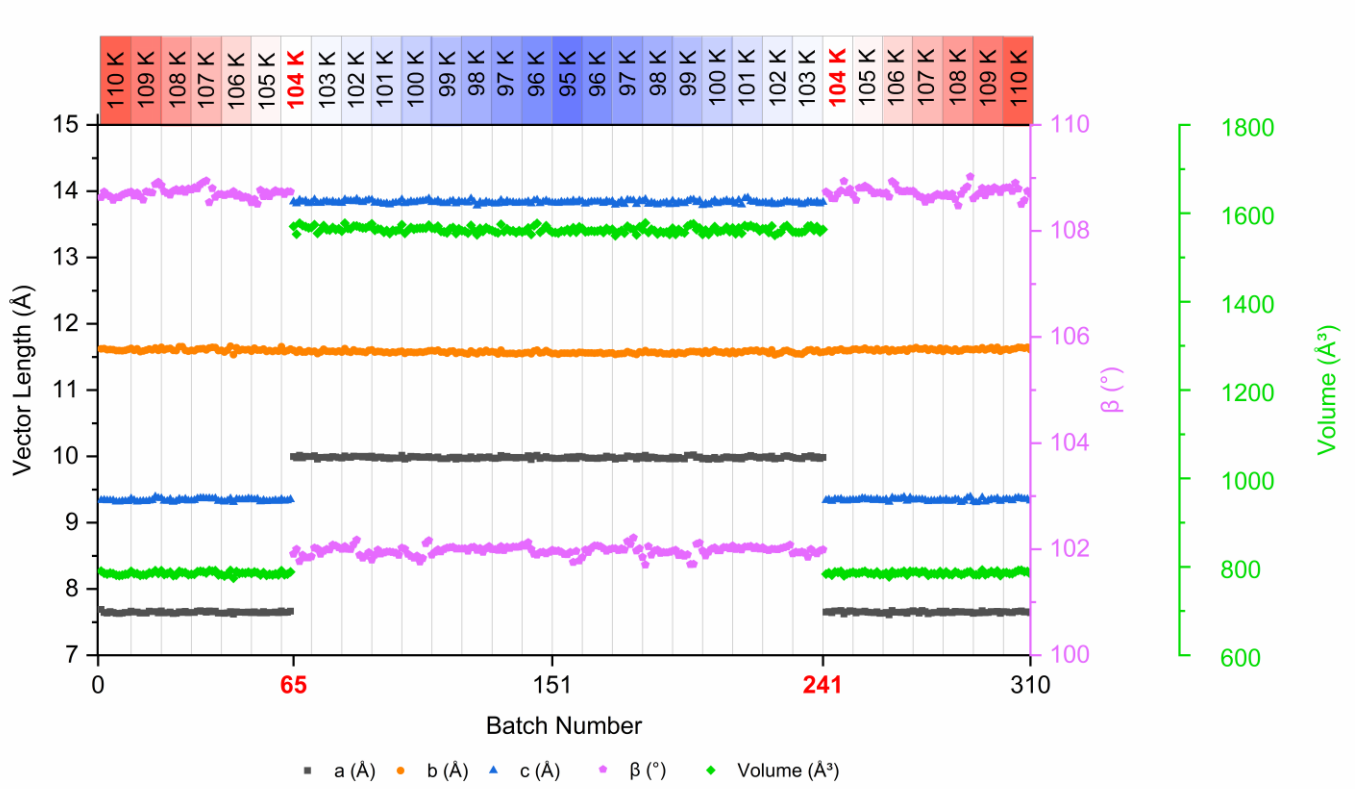

Figure 3: Dynamic *in situ* crystallographic data collected utilizing proprietary software. The unique unit cell parameters are shown. The transition can be seen occurring sharply at batch 65 while cooling and again at batch 241 while warming. Each transition occurred at 104 K. 20 frames were used in each batch for a total of 200 frames being collected at each temperature. Further details can be found in the ESI.

The assignment of $P2_1$ for LT salt was complicated by the possibility of a B-face centered cell, $B2_1$, with identical cell parameters. PLATON/ADDSYM suggests that both the large $P2_1$ and $B2_1$ cells may be reduced to a smaller $P2_1$ cell with cell parameters similar to HT Salt (Figure S22).[21-24] The $B2_1$ cell is equivalent to the reduced $P2_1$ cell with cell parameters similar to HT Salt. Notably, this suggested transformation of the larger $P2_1$ cell to the reduced $P2_1$ cell effectively alters the symmetry elements present (Figures S24-S25). For simplicity, the differences in symmetry elements present in the two possible structures will be discussed in the context of the larger $P2_1$ and $B2_1$ cells. Relative to $P2_1$, the $B2_1$ structure possesses four additional symmetry generated screw axes within the unit cell. Notably in the $B2_1$ structure, the 2,6-DHB salt former (Figures S24 and S25) resides on a screw axis and in $P2_1$ it does not. To determine if this screw axis was present, mean planes were calculated for the 2,6-DHB rings using the six carbon atoms of the benzene ring. The calculated planes indicated an offset of 9.372° between symmetry generated 2,6-DHB rings parallel to [101]; whereas a 0° offset between rings was expected and observed for the corresponding molecules in the $B2_1$ structure. Additionally, the angle between mean planes for molecules stacking parallel to [010] possessed an angle of 82.433°; whereas the same planes in the $B2_1$ structure were determined to be 82.830° (Figure S26). Also, the distance between planes along the [010] stack differed by 0.020 Å between centroids in the $P2_1$ structure. In the $B2_1$ structure the distances were equivalent due to the presence of the proper screw axes passing through the 2,6-DHB rings. The differences in 2,6-DHB mean plane distances and angles confirms the presence of two crystallographically independent 2,6-DHB molecules that are not related by a screw axis operation in $P2_1$, as would be the case for $B2_1$ symmetry. Additionally, refinement using the $P2_1$ cell setting yielded a lower R_1 value than that of the $B2_1$ cell (3.35% versus 3.67%), respectively, further supporting the assignment of $P2_1$ at temperatures between 90-104 K. Fractional atomic coordinates for the proposed $B2_1$ system can be found in Table S6.

Several geometric changes associated with the high temperature $P2_1$ to lower temperature $P2_1$ phase transition. The two crystallographically unique nicotinium molecules in **LT salt** are displaced in approximately opposite directions relative to the position of the nicotinium molecule that would be present in the $B2_1$ structure (Figure S13). Each 2,6-DHB molecule undergoes a slight rotation about its molecular C_2 axis again with opposite rotation for the two independent molecules (Figure S14).

The impact of the changes induced by the phase transition on the intermolecular contacts were determined to be minimal. Hirshfeld surface analysis of the nicotinium and 2,6-DHB molecules in each structure revealed that the interaction environment around each molecule was essentially conserved after the phase transition (Figure 2; Table S7). The API environment had fewer O-H/H-O interactions ralated to the charge transfer in contrast with the salt former environment. In addition, a larger percentage of H-N/N-H interactions were present in the API surface, as C-H---N interactions were present between adjacent nicotiniums.

Single crystal X-ray diffraction measurements performed during stepwise temperature changes were used to obtain time dependent data to determine the nature of the phase transition as well as investigate the reversibility and the temperature at which it occurs (Figure 3). Details pertaining to this method are described in the ESI. Upon cooling from 110 K, an abrupt change from the high temperature unit cell to the low temperature cell was observed at 104 K. Continued cooling to 95 K produced no additional changes in the unit cell. Upon heating from 95 K to 110 K, the until cell reverted back to the original parameters at 104 K, thus demonstrating that the phase transition occurs in a single crystal to single crystal manner and is reversible with no additional phases detected over this temperature range. Additionally, no visible damage to the crystal was observed during the course of these experiments (Figure S16).

In summary, a one-to-one stoichiometric nicotine-based crystal was synthesized using the salt former 2,6-DHBA. This salt undergoes at $P2_1$ to $P2_1$ reversible phase transition at 104 K, the first reported phase transition for a nicotine containing molecular crystal. Above 104 K the structure exhibits columns parallel to [010], which intercalate along [001] forming sheets which stacked along [100] to produce the bulk structure. Upon cooling below 104 K, the API and 2,6-DHB molecules undergo symmetry breaking translations and rotations which result an approximate doubling of the until cell. Analysis of the crystal structure and refinement parameters provided a basis for rejecting a low temperature $B2_1$ structure. The identification and characterization of phase transitions in crystalline systems, especially those intended for human consumption, is necessary for the safe and reliable use and manufacture of these materials.

Author Contributions

The authors declare no conflict of interest. The final version of this manuscript has been approved by all authors. Data curation: Devin J. Angevine, Travis B. Mitchell, Xiaotong Zhang; Formal analysis: Devin J. Angevine and Jason B. Benedict; Funding acquisition: Jason Benedict; Project administration: Jason B. Benedict; Writing – original draft: Devin Angevine and Travis B. Mitchell; Writing – review & editing: Devin J. Angevine and Jason B. Benedict.

Conflicts of Interest

The authors declare no conflicts of interest in the work. The final version of this manuscript has been approved by all authors.

References

1. K. Fagerström, *Nicotine Tob Res*, 2005, **7**, 343-350.
2. N. Borduas, J. G. Murphy, C. Wang, G. da Silva and J. P. D. Abbatt, *Environmental Science & Technology Letters*, 2016, **3**, 327-331.
3. T. A. Henry, *The Plant Alkaloids*, 4th edn., 1949.
4. E. Adamek, M. Goniewicz, W. Baran and A. Sobczak, *CHEM*, 2015, DOI: 10.5171/2015.157781, 1-5.
5. J. E. Chavarrio Cañas, M. Monge-Palacios, E. Grajales-González and S. M. Sarathy, *The Journal of Physical Chemistry A*, 2021, **125**, 3177-3188.
6. A. Pinner and R. Wolffenstein, *Berichte der deutschen chemischen Gesellschaft*, 1891, **24**, 61-67.
7. C. H. Rayburn, W. R. Harlan and H. R. Hanmer, *Journal of the American Chemical Society*, 1941, **63**, 115-116.
8. M. H. Ayad, *Drug Delivery*, 2015, **22**, 877-884.
9. R. Ghadi and N. Dand, *J. Controlled Release*, 2017, **248**, 71-95.
10. M. Karimi-Jafari, L. Padrela, G. M. Walker and D. M. Croker, *Crystal Growth & Design*, 2018, **18**, 6370-6387.
11. T. L. Rogers, J. Hu, Z. Yu, K. P. Johnston and R. O. Williams, 3rd, *Int J Pharm*, 2002, **242**, 93-100.
12. D. Capucci, D. Balestri, P. P. Mazzeo, P. Pelagatti, K. Rubini and A. Bacchi, *Cryst. Growth Des.*, 2017, **17**, 4958-4964.
13. WO2021126313A1, June 2021.
14. D. J. Angevine, K. J. Camacho, J. Rzayev and J. B. Benedict, *Crystal Growth & Design*, 2022, **22**, 1594-1603.
15. D. J. Angevine, K. J. Camacho, J. Rzayev and J. B. Benedict, *CrystEngComm*, 2022, **24**, 6155-6164.
16. D. J. Angevine, K. J. Camacho, J. Rzayev and J. B. Benedict, *Molecules*, 2022, **27**, 6853.
17. J. A. Rothwell, J. Perez-Jimenez, V. Neveu, A. Medina-Remón, N. M'Hiri, P. García-Lobato, C. Manach, C. Knox, R. Eisner, D. S. Wishart and A. Scalbert, *Database*, 2013, **2013**.
18. A. J. Cruz-Cabeza, *CrystEngComm*, 2012, **14**, 6362-6365.
19. W. Kaminsky, *Journal of Applied Crystallography*, 2005, **38**, 566-567.
20. W. Kaminsky, *Journal of Applied Crystallography*, 2007, **40**, 382-385.
21. A. Spek, *Journal of Applied Crystallography*, 2003, **36**, 7-13.
22. A. Spek, *Acta Crystallographica Section D*, 2009, **65**, 148-155.
23. A. L. Spek, *Inorganica Chimica Acta*, 2018, **470**, 232-237.
24. A. Spek, *Acta Crystallographica Section E*, 2020, **76**, 1-11.
25. G. Sheldrick, *Acta Crystallographica* Section A, 2015, **71**, 3-8.
26. G. Sheldrick, *Acta Crystallographica* Section C, 2015, **71**, 3-8.
27. O. V. Dolomanov, L. J. Bourhis, R. J. Gildea, J. A. K. Howard and H. Puschmann, *Journal of Applied Crystallography*, 2009, **42**, 339.
28. C. F. Macrae, I. Sovago, S. J. Cottrell, P. T. A. Galek, P. McCabe, E. Pidcock, M. Platings, G. P. Shields, J. S. Stevens, M. Towler and P. A. Wood, *Journal of Applied Crystallography*, 2020, **53**, 226-235.
29. Bruker (2021). *APEX4*. Bruker AXS Inc., Madison, Wisconsin, USA.
30. P. R. Spackman, M. J. Turner, J. J. McKinnon, S. K. Wolff, D. J. Grimwood, D. Jayatilaka and M. A. Spackman, *Journal of Applied Crystallography*, 2021, **54**, 1006-1011.